analytical chemistry

pubs.acs.org/ac Article

Indicator Dyes and Catalytic Nanoparticles for Irreversible Visual Hydrogen Sensing

Michael E. Smith, Angela L. Stastny, John A. Lynch, Zhao Yu, Peng Zhang,* and William R. Heineman*

Cite This: *Anal. Chem.* 2020, 92, 10651−10658 Read Online

ACCESS | Metrics & More | Article Recommendations | Supporting Information

ABSTRACT: Using ultraviolet−visible (UV−vis) absorption spectroscopy, we have tested the reactivity of various indicator molecules combined with catalytic bimetallic gold−palladium nanoparticles (Au−Pd NPs) in solution for an irreversible and visual response to H_2. Our aim was to identify the most suitable indicator/Au−Pd NP system for the future development of a thin, wearable, and visual H_2 sensor for noninvasive monitoring of *in vivo* Mg-implant biodegradation in research and clinical settings with fast response time. The indicators studied were bromothymol blue, methyl red, and resazurin, and the reactions of each system with H_2 in the presence of Au−Pd NPs caused visual and irreversible color changes that were concluded to proceed via redox processes. The resazurin/Au−Pd NP system was deemed best-suited for our research objectives because (1) this system had the fastest color change response to H_2 at levels relevant to *in vivo* Mg-implant biodegradation compared to the other indicator/Au−Pd NP systems tested, (2) the observed redox chemistry with H_2 followed well-understood reaction pathways reported in the literature, and (3) the redox products were nontoxic and appropriate for medical applications. Studying the effects of the concentrations of H_2, Au−Pd NPs, and resazurin on the color change response time within the resazurin/Au−Pd NP system revealed that the H_2-sensing elements can be optimized to achieve a faster or slower color change with H_2 by varying the relative amounts of resazurin and Au−Pd NPs in solution. The results from this study are significant for future optical H_2 sensor design.

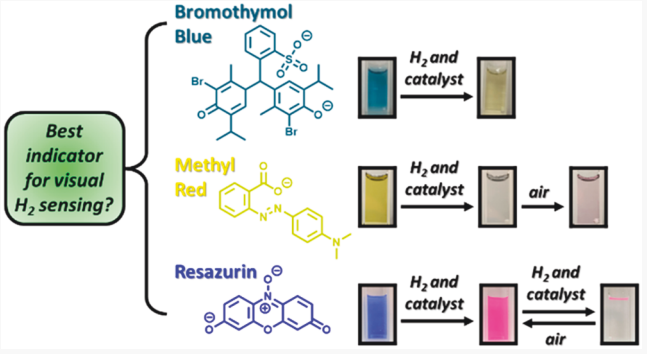

Magnesium (Mg) and its alloys have the capability of outperforming traditionally used materials for orthopedic applications such as bone repair because they can act as load-bearing implants that safely biodegrade when no longer needed.[1−11] We have previously shown that an appreciable fraction of the hydrogen gas (H_2) liberated as a corrosion product from Mg-implant biodegradation can be detected transdermally and noninvasively at levels ranging from ∼30 to ∼700 μM by placing electrochemical or visual H_2 sensors on mouse skin directly above implants as they biodegraded *in vivo*.[2,5,6,12] These noninvasive H_2-sensing methods are considered to be fast, reliable, and accurate representations of the extent of *in vivo* Mg-implant biodegradation, since the measured H_2 levels correlated nicely with the biodegradation rates measured via the highly accurate mass loss method of explanted implants.[2,5] These significant discoveries opened the door to using H_2-sensing as a platform for monitoring the *in vivo* biodegradation of Mg-implants by a simple, noninvasive procedure without exposure to X-rays. Furthermore, this sensing platform enables *in vivo* biodegradation to be measured in real-time. These features are desirable in medical research settings in which new biodegradable materials and devices are developed and in clinical settings for the routine evaluation of patients with Mg-implants. However, the sensors used in the aforementioned studies are limited for monitoring H_2 in such settings. For example, the electrochemical H_2 sensor offers remarkable sensitivity, yet the sensor itself and the associated instrumentation are costly, complex, and require a reasonable skill level for proper use. This sensor also requires regular calibration and tedious multiple measurements if mapping of H_2 levels over an area above an implant is desired, since the sensor surface is ∼50 μm in diameter. The visual H_2 sensor of ∼10 μm thickness and ∼1 cm^2 surface area afforded detailed mapping of H_2 levels above implants, which is a very useful tool for monitoring larger implants such as plates, and the H_2 detection could be made easily using a cell phone.[5,12] However, the exposure times required to induce detectable color changes were on the order of hours, which limit its practical use. To circumvent these problems, the objective of this research was to test the reactivity of various indicator

Received: April 24, 2020
Accepted: July 6, 2020
Published: July 6, 2020

https://dx.doi.org/10.1021/acs.analchem.0c01769
Anal. Chem. 2020, 92, 10651−10658

molecules combined with catalytic bimetallic gold−palladium nanoparticles (Au−Pd NPs) in solution for irreversible and visual response to H_2 with the aim to later develop the most suitable indicator/Au−Pd NP system into a thin, wearable, and optical H_2-sensing device for noninvasive monitoring of *in vivo* Mg-implant biodegradation in medical research and clinical settings with fast response time.

Nanoparticles (NPs), such as those of platinum (Pt),[13−17] palladium (Pd),[5,11,18−20] and Au−Pd,[21−25] have attracted considerable interest for use in a variety of H_2-sensing platforms and applications due to their unique catalytic abilities. Our basis for choosing Au−Pd NPs for our research objectives stems from reports describing how alloys containing Au and Pd are particularly advantageous for H_2-sensing and exhibiting enhanced H_2 adsorption and solubility.[26,27] With respect to signal transduction for H_2-sensing, catalytic NPs have been combined with different indicators for the development of optical H_2 sensors in which the sensing mechanism relies on the dissociation of H_2 at the NP surface to form highly reactive hydrogen atoms that subsequently undergo a redox reaction with an indicator to cause a visual color change.[5,13] For example, Seo et al.[13] used a reagent containing methylene blue and Pt NPs to quantify the amount of H_2 dissolved in water as the reagent underwent a blue to colorless transition upon reaction with H_2. Although this simple method was shown to be as effective as an electrochemical sensor for H_2 quantification,[13] the use of methylene blue as a H_2-sensing molecule is disadvantageous for certain applications because the reduction of methylene blue and the subsequent color change are known to be reversible in the presence of oxygen (O_2).[28] Regarding our goal of future optical H_2 sensor development for monitoring Mg-implant biodegradation *in vivo*, the sensing mechanism should ideally be an irreversible process such that the sensor color change resulting from redox reactions between hydrogen atoms, formed at the NP catalyst surface, and indicator molecules cannot be reverted back to the original sensor color by O_2. An optical H_2 sensor with irreversible capabilities would likely achieve the lower limits of detection needed for medical applications, since O_2 would not affect the overall color change response time of the sensor. From a practical perspective, our developed optical H_2 sensor should also exhibit a color change response on the order of ∼10 min. Therefore, the primary goal of this work was to investigate various indicators that could undergo irreversible color changes upon reaction with H_2 at levels relevant to *in vivo* Mg-implant biodegradation (e.g., ∼ 30 to ∼700 μM) in the presence of Au−Pd NP catalysts and to identify the most suitable indicator/Au−Pd NP system for future optical H_2 sensor development by comparing the color change response time of each system.

The specific indicators investigated in this study were those shown in Figure 1 and included bromothymol blue, methyl red, and resazurin. Bromothymol blue (Figure 1A) is a well-known acid/base indicator that exhibits a blue to yellow color change upon protonation.[29] Methyl red (Figure 1B) is another well-known acid/base indicator that has yellow and red colors in the deprotonated and protonated forms, respectively.[30] Due to the reported electrochemical reduction pathways in the literature for these molecules,[31−33] it was hypothesized that bromothymol blue and methyl red could undergo rapid and irreversible reduction reactions with H_2 in the presence of Au−Pd NP catalysts that would result in visual color changes through a similar mechanism described by Seo et al.[13] for the methylene blue/Pt NP system. Resazurin (Figure 1C), a common redox indicator that exhibits a blue color at neutral pH, can undergo an irreversible reduction to lose water to form a pink-colored and highly fluorescent resorufin product.[34−38] A subsequent reduction of resorufin to the colorless dihydroresorufin can occur, but the process is reversible in the presence of O_2.[35] Despite the reversibility of this subsequent reaction, resazurin was hypothesized to be a good candidate for our research objectives, since the initial irreversible reduction that forms the highly luminescent resorufin product would likely be the only color transition observed at low levels of H_2 exposure, and this product could serve nicely as the analytical signal. Furthermore, previous work has shown that resazurin can be converted to resorufin upon reaction with H_2 in the presence of Pt NP catalysts.[39]

In this work, we tested the reactivity of H_2 with bromothymol blue, methyl red, and resazurin indicators combined with Au−Pd NP catalysts by preparing buffered solutions (pH ∼7.5) and exposing each to H_2 at a known flow rate and concentration while ultraviolet−visible (UV−vis) absorption spectra were monitored over time. The indicator/Au−Pd NP system most suitable for our target application for future optical H_2 sensor development was identified by comparing the changes in the characteristic UV−vis absorption maxima of each indicator/Au−Pd NP system as a function of H_2 exposure time. The most suitable indicator/Au−Pd NP system was further studied via UV−vis spectroscopy to examine the effects of varying the concentrations of H_2, Au−Pd NPs, and indicator on the color change response time.

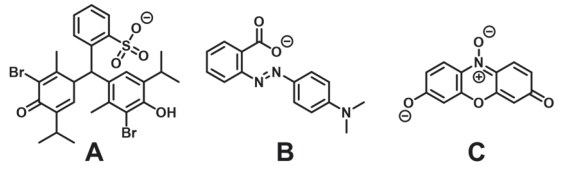

Figure 1. Anions of the sodium salts of (A) bromothymol blue, (B) methyl red, and (C) resazurin.

EXPERIMENTAL SECTION

Chemicals, Materials, and Instrumentation. All chemicals and materials were used as received. Resazurin sodium salt ($C_{12}H_6NNaO_4$, >85.0% by HPLC) was purchased from TCI America Inc. Sodium salts of methyl red ($C_{15}H_{14}N_3NaO_2$) and bromothymol blue ($C_{27}H_{27}Br_2NaO_5S$) were acquired from ACROS Organics. Gold(III) chloride trihydrate ($HAuCl_4{\cdot}3H_2O$, ≥99.9% trace metal basis), and potassium hexachloropalladate(IV) (K_2PdCl_6, 99%) were purchased from Sigma-Aldrich. Trisodium citrate dihydrate ($Na_3C_6H_5O_7{\cdot}2H_2O$), phosphate-buffered saline (PBS, 10× solution, pH 7.4), and a three-way valve of polytetrafluoroethylene (PTFE) were obtained from Fisher Scientific. Hydrion pH paper (0−13 range) was obtained from Grainger. All aqueous solutions were prepared using deionized water (≥18 MΩ·cm, referred to as DI water herein). Ultrahigh purity grades of H_2 and N_2 gases were obtained from Wright Brothers Inc. A gas proportioning rotameter (#GMR2−010343) equipped with two flow tubes (FL-2GP-61C-61C) was purchased from Omega Engineering. A rotameter with a single flow tube (#FP 1/8-038-G-6) was acquired from Lab-Crest, Fisher & Porter Co. Tygon tubing (1/4" i.d., 1/2" o.d.) was purchased from McMaster-Carr. Hypodermic needles

https://dx.doi.org/10.1021/acs.analchem.0c01769
Anal. Chem. 2020, 92, 10651−10658

(305120-23G) were acquired from BD Co. Stainless steel tubing (1/8" o.d.) was purchased from Supelco. An amperometric H_2 sensor (H_2-NP-705273) and multimeter were obtained from Unisense. A DryCal DC-Lite flow calibrator was acquired from Brandt Instruments, Inc. Microcentrifuge tubes were purchased from Avant. NPs were centrifuged using a Sorvall Legend Micro 21. UV−vis spectra of all samples were collected using a USB4000 UV−vis spectrophotometer (Ocean Optics) by loading samples into a standard quartz cuvette of 1 cm path length. For all time-based UV−vis spectra, data shown at $t \geq 0$ s correspond to gas being delivered into samples, while data at $t < 0$ s correspond to no gas being delivered into samples. Transmission electron microscopy (TEM) measurements of NP samples were performed on a Biotwin 12 TEM (FEI) by depositing a drop of solution on a Formvar-covered, carbon-coated copper grid (Electron Microscopy Sciences) and letting the solvent dry at room temperature. Size distributions, average hydrodynamic diameters ($\tilde{d}$), and zeta-potentials (ζ) of NP samples were measured using dynamic light scattering (DLS) instrumentation (Microtrac).

Synthesis of Au−Pd Bimetallic Nanoparticle Master Solution. Au−Pd NPs were synthesized by the coreduction of $[AuCl_4]^-$ and $[PdCl_6]^{2-}$ ions via trisodium citrate as described previously with slight modifications.[40] A batch of Au−Pd NP solution was prepared by gently boiling and vigorously stirring a solution containing 312 μL of 20 mM $HAuCl_4 \cdot 3H_2O$ and 312 μL of 20 mM K_2PdCl_6 at a total volume of 50.00 mL in DI water. Three milliliters of 2% (m/V) trisodium citrate was added quickly, and the solution was left to boil under vigorous stirring for 15 min. The solution was then cooled to room temperature before being stored in the dark at ∼4 °C until further use. A total of five batches of Au−Pd NPs were prepared and combined in the following way to make a highly concentrated Au−Pd NP master solution. First, the contents of the five batches were transferred to one borosilicate Erlenmeyer flask and boiled, uncovered, under vigorous stirring until the solvent level reached ∼25 mL. This solution was left to cool to room temperature, and the contents were transferred into several microcentrifuge tubes and centrifuged at 14,000 rpm for 20 min. The supernatants were discarded as waste while the pellets of Au−Pd NPs remained in the bottom of each tube. All pellets were sonicated, creating highly concentrated microvolumes of Au−Pd NPs, and combined into a borosilicate glass container, thereby creating a highly concentrated solution of Au−Pd NPs with a volume of ∼5.00 mL in DI water. This solution will be referred to as the Au−Pd NP master solution herein.

Gas Flow Setups and Determining the Concentration and Flow Rate of H_2 Delivered to Samples. The general gas flow setup for various experiments is depicted in Figure S1 of the Supporting Information (SI). Using appropriate fittings and stainless-steel tubing, H_2 and N_2 gas tanks were fitted with regulators and then connected to the inlets of a gas proportioning rotameter (GPR) containing two separate flow tubes for H_2 and N_2 (labeled "GPR-H_2" and "GPR-N_2" in Figure S1, SI). Varying the flow rates of H_2 and N_2 in the GPR flow tubes permitted the ability to make a sample mixture of H_2/N_2 gas at a particular volume to volume ratio (v/v) based on the respective GPR flow tube scale readings. The outlet of the gas proportioning rotameter was connected to a rotameter equipped with a single flow tube to allow controlled flow of the sample gas. The outlet of this flow tube was then connected to a three-way valve via stainless steel and Tygon tubings. Lastly, stainless steel tubing was connected to the remaining outlets of the three-way valve to allow directional flow of the sample gas to vent or to an experiment at a controlled rate. Flow rate data of N_2 and H_2 gases from the GPR flow tubes at various scale readings were provided by Omega Engineering (Table S1, SI), and plots of the gas flow rate (mL/min) vs rotameter scale reading (mm) were made for each gas and fit to quadratic equations (Figure S2, SI). To create a H_2/N_2 gas mixture with a desired volume percentage of H_2 ($\%V_{H_2,theoretical}$), a reasonable flow rate of H_2 at the GPR flow tube (GPR:H_2 flow rate) was chosen. Equation S1 (SI) was then used to calculate the necessary flow rate of N_2 at the GPR flow tube (GPR:N_2 flow rate) that would achieve the desired value of $\%V_{H_2,theoretical}$. To determine the precise GPR flow tube scale readings for H_2 and N_2 that would achieve the desired $\%V_{H_2,theoretical}$, the flow rates (y-values) for the respective gases were plugged into the corresponding quadratic equations from Figure S2 (SI) to solve for the scale readings (x-values).

To deliver gas at a known rate to an experiment from the single flow tube rotameter, this flow tube needed to be calibrated. This was accomplished by using a DryCal DC-Lite flow calibrator for pure N_2 and measuring the flow rate at various scale readings. It was deemed unsafe to measure H_2 flow in either pure or mixed forms using the DryCal DC-Lite flow calibrator due to potential sparking hazards. Thus, flow rates of pure H_2 coming from the single flow tube rotameter at various scale readings were calculated theoretically using eq S2 (SI) where R, Q, and ρ represent the rotameter scale reading (mm), volumetric flow rate (mL/min), and gas density (g/L).[41] The gas densities of pure N_2 and H_2 used were 1.25 g/L and 0.09 g/L, respectively, and were determined using the ideal gas law at standard temperature and pressure. When comparing flow rates for two gases at the same rotameter scale reading (i.e., where $R_1 = R_2$), eq S2 (SI) reduces to eq S3 (SI).[41] The rotameter calibration for N_2 could therefore be applied to pure H_2 using eq S3 (SI).[41] The measured flow rates for pure N_2 and calculated flow rates of pure H_2 at various scale readings are summarized in Table S2 (SI).

For flow rate determinations of H_2/N_2 gas mixtures, it was necessary to measure the concentration of H_2 within the mixture using an amperometric H_2 sensor to calculate theoretical gas densities. To do so, an amperometric H_2 sensor was calibrated as described previously.[1,5,6] The sensor was connected to a multimeter and polarized at +1000 mV for at least 1 h before use. Pure H_2 was delivered into ∼20 mL of DI water at 257 mL/min for 30 min to form a 100% saturated H_2 solution constituting an 800 μM concentration at room temperature.[1,2,5,6] From this stock solution, standards of 0, 8, 40, 100, 200, 400, and 600 μM were prepared via dilution with DI water. The amperometric H_2 sensor tip was immersed in each standard, and six measurements of the steady-state current were taken after at least 2 min to generate a current vs H_2 concentration calibration curve (Figure S3, SI). After calibrating the amperometric H_2 sensor, the scale readings of GPR-H_2 and GPR-N_2 flow tubes were set to the desired levels to form a H_2/N_2 gas mixture with defined volume percentages of H_2 ($\%V_{H_2}$) and N_2 ($\%V_{N_2}$). The H_2 concentration of a H_2/N_2 gas mixture was measured using the apparatus in Figure S4 (SI). Two milliliters of DI water was placed in a 1 × 1 cm^2 glass vessel and clamped to a support stand. A needle connected to the gas flow apparatus was inserted into the

https://dx.doi.org/10.1021/acs.analchem.0c01769
Anal. Chem. 2020, 92, 10651−10658

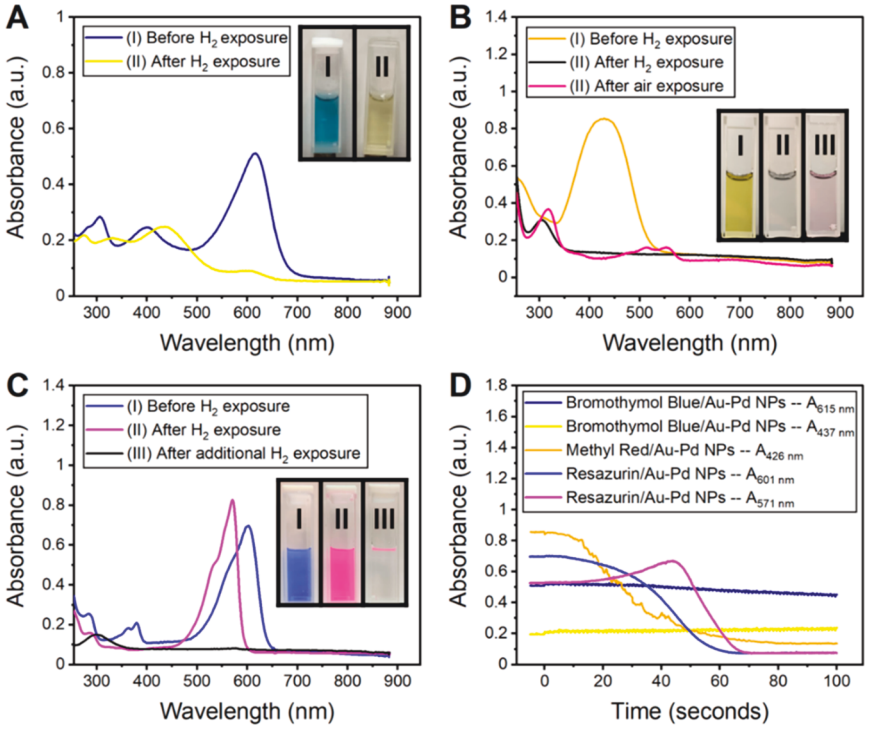

Figure 2. Comparison of the color changes observed for various indicator/Au−Pd NP systems upon reaction with 800 μM H_2. Raw UV−vis spectra are shown in parts A−C. (A) The bromothymol blue/Au−Pd NP system before (navy blue trace) and after 20 min of H_2 exposure (yellow trace). (B) The methyl red/Au−Pd NP system before (brownish yellow trace) and after 2 min of H_2 exposure (black trace), followed by exposure to air for 10 min (red trace). (C) The resazurin/Au−Pd NP system before (blue trace) and 1 min after exposure to H_2 (pink trace), followed by additional H_2 exposure for 2 min (black trace). Inset photographs in parts A−C are the sample solution colors observed during the experiment. (D) Comparison of the real-time changes in the characteristic UV−vis absorption bands for each indicator/Au−Pd NP system as a function of H_2 exposure time.

water. H_2/N_2 gas was delivered into the water for 20 min by setting the single flow tube rotameter scale reading to 15.00 mm to saturate the solution. The gas flow to the sample was cut off and the H_2 concentration (in μM) was measured by inserting the calibrated amperometric H_2 sensor into the sample and covering the glass vessel with a Teflon cap that had the corner sectioned off. The volume percentage of H_2 ($\%V_{H_2}$) in the H_2/N_2 mixture was calculated according to eq S4 (SI), where $[H_2]_{measured}$ was the electrochemically measured μM concentration of H_2 in the H_2/N_2 mixture, and $[H_2]_{saturated}$ was the saturated concentration of H_2 in water, which is 800 μM at room temperature and standard pressure.[1,6,13] The volume percentage of N_2 ($\%V_{N_2}$) in the H_2/N_2 mixture was calculated according to eq S5 (SI). The theoretical density of the H_2/N_2 mixture (ρ_{mix}) was calculated via eq S6 (SI), where MW_{H_2} and MW_{N_2} are the molecular weights of H_2 and N_2, respectively. Once ρ_{mix} was known, this value was plugged into eq S7 (SI) to calculate the flow rate of the H_2/N_2 mixture (Q_{mix}) at a particular flow tube rotameter scale reading using the calibrated flow of N_2 (Q_{N_2}) from Table S2 (SI). Three different H_2/N_2 mixtures were made according to the data shown in Table S3 (SI). From the data in Table S3 (SI), the flow rates of these sample gases were calculated using eq S7 (SI) at various single flow tube rotameter scale readings, and the results are summarized in Table S4 (SI). Plots of flow rate vs scale reading were made for each gas listed in Table S4 (SI), and the results are shown in Figure S5 (SI). Quadratic functions were fit to the data in Figure S5 (SI) and were then used to calculate the necessary single flow tube rotameter scale reading to deliver sample gas at a 23.40 mL/min flow rate during an experiment. This flow rate was used for all experiments described herein.

Testing Various Indicator/Au−Pd NP Systems for Visual Color Change upon Reaction with H_2. Aqueous solutions of bromothymol blue, methyl red, and resazurin indicators were prepared in volumetric flasks in 1× PBS buffer and had an indicator concentration of 20 μM and Au−Pd NPs present at 0.8% (v/v). The samples were then exposed to 800 μM H_2 using the apparatus shown in Figure S6 (SI) as UV−vis absorption spectra of all samples were collected over time.

The Resazurin/Au−Pd NP System: Effects of the Concentrations of H_2, Au−Pd NPs, and Resazurin on the Color Change Response Time. The effects of the concentrations of H_2, Au−Pd NPs, and resazurin on the response time of observed color changes within resazurin/Au−Pd NP systems were studied using the apparatus in Figure S6 (SI). In all experiments, 1× PBS buffer was used as the solvent. To study H_2 concentration effects, three identical samples were prepared that had 20 μM resazurin concentrations and Au−Pd NPs present at 0.8% (v/v). These samples were then exposed to H_2 at 800, 558, and 169 μM concentrations. The effects of Au−Pd NP concentration were studied by preparing two samples with resazurin concentrations of 20 μM. Each sample differed in the v/v percentage of Au−Pd NPs present in solution, and the amounts used were 2% and 0.8%. Each sample was then exposed to 800 μM H_2. The effects of resazurin concentration were studied by preparing three samples with Au−Pd NPs at 0.8% (v/v), varying the resazurin

https://dx.doi.org/10.1021/acs.analchem.0c01769
Anal. Chem. 2020, 92, 10651−10658

concentrations at 5, 20, and 40 μM, and then exposing each sample to 800 μM H_2.

The Resazurin/Au−Pd NP System: Control Experiments. To elucidate the cause of the observed color changes in the resazurin/Au−Pd NP system, a series of control experiments were performed by flowing pure H_2 or N_2 gases into various sample combinations (Table S5, SI) using the apparatus described in Figure S6 (SI). To ensure that the UV−vis absorption signal remained stable during the data collection interval, a sample of resazurin/Au−Pd NPs was placed in a cuvette and monitored without any gas flow (experiment 1, Table S5, SI). Gold colloidal nanoparticles (Au NPs) of ∼25 nm size were synthesized as described previously[42] to examine if Au had any catalytic effect on the reduction of resazurin by H_2. A master solution of Au NPs was prepared in a similar fashion as described for the Au−Pd NP master solution, except that the centrifugation conditions were 7,000 rpm for 10 min. A series of controls using N_2 (experiments 2−7) and H_2 (experiments 8−12) were then conducted (Table S5, SI). Samples containing resazurin had 20 μM concentrations. Samples containing NPs had 0.8% (v/v) concentrations.

RESULTS AND DISCUSSION

Characterization of Au−Pd and Au NPs. UV−vis, TEM, and DLS instrumentation were used to characterize the Au−Pd and Au NPs (Figure S7, SI). UV−vis spectra of the as-synthesized NP solutions of Au−Pd and Au exhibited bands at ∼520 and ∼525 nm, respectively (Figure S7A, SI). These bands were attributed to the localized surface plasmon resonance of the Au material within the nanostructures.[43] NPs are known to aggregate in high salt concentrations,[44] and this phenomenon can be seen when samples at 0.8% v/v concentrations were dispersed in buffer (Figure S7A, dashed lines, SI). The average hydrodynamic diameters ($\tilde{d}$) of the Au−Pd and Au NPs were 18.4 and 24.9 nm, respectively (Figures S7D and S7E, SI).

Comparisons of the Visual Color Changes of Various Indicator/Au−Pd NP Systems upon Reaction with H_2. All indicator/Au−Pd NP systems underwent irreversible and visual color changes upon reaction with H_2 (Figure 2A−C). One reaction pathway involving a blue to yellow color transition was observed for the bromothymol blue/Au−Pd NP system upon H_2 exposure for 20 min (inset photographs in Figure 2A). UV−vis absorption spectra of this sample before (navy blue trace) and 20 min after (yellow trace) H_2 exposure revealed maxima at ∼615 and ∼437 nm, respectively (Figure 2A). These values agree nicely with those reported in the literature for the protonated and deprotonated forms of pure bromothymol blue.[29] However, the observed color changes in Figure 2A were attributed to a redox reaction rather than an acid/base reaction, since the solution pH was maintained at neutral throughout the experiment.

For the methyl red/Au−Pd NP system, three colors were observed (inset photographs of Figure 2B) and had reaction pathways that proceeded from yellow to colorless during 2 min of H_2 exposure and then colorless to faint red after exposure to ambient air for 10 min. Similarly, the yellow to colorless transition of the methyl red/Au−Pd NP system upon reaction with H_2 was attributed to a redox reaction rather than an acid/base reaction, since the solution pH did not change throughout the H_2 exposure. UV−vis absorption spectra of the various sample colors observed for the methyl red/Au−Pd NP system before (brownish yellow trace) and 2 min after (black trace) H_2 exposure revealed maxima at ∼430 and ∼305 nm, respectively, while the sample after 10 min of air exposure had a maximum at ∼316 nm with additional bands at ∼514, ∼552, and ∼700 nm (Figure 2B).

The resazurin/Au−Pd NP system also displayed visual color changes upon reaction with H_2, and these data are displayed in Figure 2C. Three colors were observed during the experiment (inset photographs of Figure 2C) and included reaction pathways that went from blue to pink after 1 min of H_2 exposure, from pink to colorless after additional H_2 exposure for 2 min, and then colorless to pink after exposure to ambient air. These color changes were attributed to the redox reaction described in Figure 3, in which resazurin (blue color)

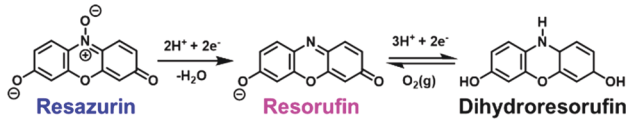

Figure 3. Redox reactions of resazurin upon reaction with H_2 in the presence of Au−Pd NP catalysts at pH ∼7.5.

underwent an irreversible reduction in the presence of H_2 and Au−Pd NP catalysts to form resorufin (pink color) with a subsequent reduction to dihydroresorufin (colorless) that was reversible in the presence of ambient O_2.[34−36,38] These observations were supported by the spectral data in Figure 2C. For example, the UV−vis absorption maxima for the resazurin/Au−Pd NP sample before (blue trace) and after (pink trace) H_2 exposure were ∼601 and ∼571 nm, respectively (Figure 2C). These maxima agree nicely with those reported in the literature for pure resazurin and resorufin at comparable pH.[37] The redox reaction reversibility of dihydroresorufin back to resorufin in the presence of ambient O_2 is well-known[35] and can be seen visually in the third photograph in the inset of Figure 2C. This photograph was taken after converting the sample to the colorless form via H_2 exposure and then exposing it to ambient air for ∼2 min. A small layer of pink color, corresponding to resorufin, formed at the solution/air interface shortly after exposure to ambient air, demonstrating that dihydroresorufin is very sensitive to O_2. The colorless solution eventually reverted back to a full pink color after ∼30 min of air exposure. Like the other indicator/Au−Pd NP systems investigated, the pH of the resazurin/Au−Pd NP system did not change throughout experimentation with H_2.

The characteristic UV−vis absorption maxima of all indicator/Au−Pd NP samples as a function of H_2 exposure time are displayed in Figure 2D. It is evident from these data that the bromothymol blue/Au−Pd NP system had a much slower color change response to H_2 compared to the other systems investigated, since the disappearance of the blue color and formation of the yellow color (navy blue and yellow traces in Figure 2D, respectively) did not change significantly after 100 s of H_2 exposure. These results suggest that much longer exposure times would be required to induce a detectable color change. Therefore, bromothymol blue would not be a practical indicator for future H_2 sensor development for our target application. The methyl red/Au−Pd NP system had relatively fast color change response to H_2, since the UV−vis absorption maximum corresponding to the yellow form of methyl red (brownish yellow trace in Figure 2D) decreased quickly during H_2 exposure. With respect to redox reactions, researchers have

https://dx.doi.org/10.1021/acs.analchem.0c01769
Anal. Chem. 2020, 92, 10651−10658

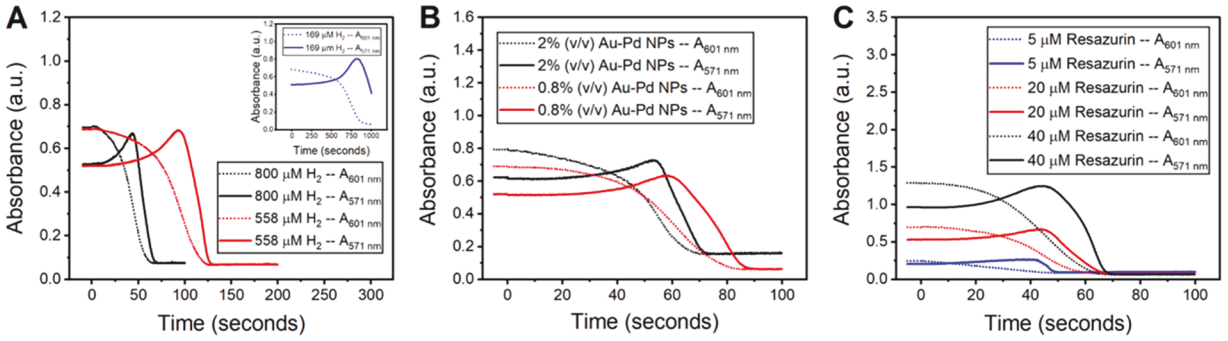

Figure 4. Effects of the concentrations of (A) H_2, (B) Au−Pd NPs, and (C) resazurin on the color change response time of the resazurin/Au−Pd NP system. The bands corresponding to resazurin (dashed lines) and resorufin (solid lines) were monitored over time during H_2 exposure.

shown that methyl red can electrochemically undergo an irreversible reduction to form anthranilic acid and *N*,*N*-dimethyl-*p*-phenylenediamine as products,[32,33] of which the latter product is known to exhibit acute toxicity.[45] Consequently, methyl red would not be used as an indicator for our research objectives in order to avoid toxic chemicals that would be problematic for medical applications. The resazurin/Au−Pd NP system also displayed a fast color change response to H_2, since the resazurin band (blue trace in Figure 2D) sharply declined while the resorufin band (pink trace in Figure 2D) increased to a maximum and eventually flatlined as H_2 was further introduced into the system and all molecules were converted to dihydroresorufin.

Of the three systems we examined, the resazurin/Au−Pd NP system was best-suited for our research objective of future optical H_2 sensor development because (1) this system had a fast color change response to H_2 compared to the other indicator/NP systems tested, (2) resazurin has well-studied reduction pathways that involve an initial irreversible reduction to a highly luminescent resorufin product, and (3) the reactants and products involved in the overall redox processes are nontoxic and appropriate for medical applications. For these reasons, the effects of the concentrations of H_2, Au−Pd NPs, and resazurin on the response time of the observed color changes within the resazurin/Au−Pd NP system were studied.

The Resazurin/Au−Pd NP System: Effects of the Concentrations of H_2, Au−Pd NPs, and Resazurin on the Color Change Response Time. The effects of H_2 are shown in the time-based UV−vis absorption spectra of resazurin/Au−Pd NP systems exposed to H_2 at 169, 558, and 800 μM concentrations (Figure 4A). These data illustrate how decreasing the H_2 concentration exposed to a resazurin/Au−Pd NP system decreased the color change response time. For example, when monitoring the resazurin bands over time (dashed line traces in Figure 4A), these bands flatlined after ∼65, 125, and 1000 s of H_2 exposure for the experiments at 800, 558, and 169 μM H_2 concentrations, respectively. Similarly, the peaks corresponding to resorufin (solid line traces in Figure 4A) reached maxima after ∼50, 100, and 800 s of H_2 exposure for the experiments at 800, 558, and 169 μM H_2 concentrations, respectively.

The effects of the concentration of Au−Pd NPs on the resazurin/Au−Pd NP system are shown in Figure 4B. Comparing the resazurin bands (dashed line traces in Figure 4B), the sample containing 2% (v/v) Au−Pd NPs flatlined at ∼70 s, while the sample containing 0.8% (v/v) Au−Pd NPs flatlined at ∼90 s. Comparing the resorufin bands (solid line traces in Figure 4B), the sample containing a larger amount of Au−Pd NPs reached a maximum at ∼54 s, while the sample containing a lower amount of Au−Pd NPs reached a maximum at ∼58 s. These data show how increasing the concentration of Au−Pd NPs within the resazurin/Au−Pd NP system decreased the color change response time upon reaction with H_2.

The effects of the concentration of resazurin on the resazurin/Au−Pd NP system are shown in Figure 4C. It is evident from these data that the sample containing the lower concentration of resazurin (blue traces in Figure 4C) underwent a faster color change, since the resazurin band (blue dashed line trace in Figure 4C) flatlined much earlier compared to the other samples and the resorufin band (blue solid line trace in Figure 4C) reached a maximum earlier than the other samples. The data obtained in this section demonstrate that the resazurin/Au−Pd NP system is viable for the future development of optical H_2 sensors for our target application because the system quickly changed color upon reaction with H_2 at levels relevant to *in vivo* Mg-implant biodegradation on a practical time scale, and the H_2-sensing elements can be optimized to achieve a faster or slower color change response to H_2 by varying the relative amounts of resazurin and Au−Pd NPs.

The Resazurin/Au−Pd NP System: Control Experiments. From the set of control experiments described in Table S5 (SI), it was observed that the UV−vis absorption bands in experiment 1 were very stable and remained nearly constant across the visible wavelength range during measurement with no gas flow (Figure S8, SI). Similar results were observed in experiments 2−7 (Table S5, SI) as N_2 was delivered into solutions (Figure S9, SI). By comparison, flowing H_2 in experiments 8−11 (Table S5, SI) gave the same lack of spectral change until both resazurin and AuNPs were present, as shown in Figure S10 (SI). These observations confirm that N_2 had no effect on the observed color changes for the resazurin/Au−Pd NP system and that color changes only arose when H_2 reacted with resazurin in the presence of Au−Pd and Au NP catalysts. For example, exposure of H_2 in experiment 12 (Table S5, SI) to the sample containing resazurin and Au NPs led to dramatic UV−vis spectral changes as the peaks corresponding to resazurin and resorufin increased and decreased, respectively (Figures S10E and S11, SI). These results show that the Au NPs catalyzed the reduction of resazurin by H_2 to form resorufin, and it has been shown in the literature that Au can catalyze the dissociation of molecular H_2 into hydrogen atoms.[46,47] Comparing the color change response times of the resazurin/Au NP (Figure S11, SI) and resazurin/Au−Pd NP systems (Figure 2D), the system

https://dx.doi.org/10.1021/acs.analchem.0c01769
Anal. Chem. 2020, 92, 10651−10658

containing Au−Pd NPs underwent faster color changes. This result was attributed to the presence of Pd in the nanostructures. Pd NPs have been shown to be more effective catalysts for H_2 sensing than those of Au.[48] Also, Au−Pd alloys have been shown to exhibit accelerated H_2 adsorption compared to Pd.[26] The resazurin/Au NP sample could not be converted to the colorless form, even after 10 min of H_2 exposure (data not shown), while the resazurin/Au−Pd NP system was fully converted to the colorless form after ∼65 s of H_2 exposure (Figure 2D). These results highlight the importance of Pd on the overall color change response time of the resazurin/Au−Pd system upon reaction with H_2.

CONCLUSIONS

We have studied various indicator/Au−Pd NP systems that are potentially useful for a variety of optical H_2-sensing applications, since each system underwent visible and irreversible color changes upon reaction with H_2 in the presence of Au−Pd NP catalysts in solution. The indicators studied were bromothymol blue, methyl red, and resazurin, and the reactions of each system with H_2 in the presence of Au−Pd NPs were concluded to proceed via redox processes. The resazurin/Au−Pd NP system was deemed best-suited for our target application of future optical H_2 sensor development for noninvasive monitoring of *in vivo* Mg-implant biodegradation in medical research and clinical settings because (1) this system had a fast color change response to H_2 compared to the other indicator/Au−Pd NP systems tested, (2) resazurin has well-studied reduction pathways that involve an initial irreversible reduction to a highly luminescent resorufin product, and (3) the reactants and products involved in the overall redox processes are nontoxic and appropriate for medical applications. Studying the effects of the concentrations of H_2, Au−Pd NPs, and resazurin on the color change response time within the resazurin/Au−Pd NP system revealed that the sensing elements can be optimized to achieve a faster or slower color change with H_2 by varying the relative amounts of resazurin and Au−Pd NPs.

The other indicator/Au−Pd NP systems were deemed unsuitable and impractical for our research objectives because the system involving bromothymol blue exhibited a relatively slow color change upon exposure to H_2, and the system involving methyl red presumably formed a redox product with acute toxicity (i.e., *N*,*N*-dimethyl-*p*-phenylenediamine). Both the color change response time and the H_2 concentration range tested for the resazurin/Au−Pd NP system are appropriate for our intended application of monitoring the biodegradation of Mg-implants used for bone repair and other medical procedures.

Although this research was driven by our interest in developing better H_2 sensors for noninvasive monitoring of *in vivo* biodegradation of Mg-based implants, the materials explored here are potentially useful for other H_2-sensing applications wherever H_2 is used.

ASSOCIATED CONTENT

Supporting Information

The Supporting Information is available free of charge at https://pubs.acs.org/doi/10.1021/acs.analchem.0c01769.

Figures, tables, and equations describing various gas flow setups and determinations of flow rates of N_2, H_2, and H_2/N_2 gases; UV−Vis, TEM, and DLS characterizations of Au−Pd and Au NPs; and UV−vis spectra of control experiments (PDF)

AUTHOR INFORMATION

Corresponding Authors

Peng Zhang − *Department of Chemistry, University of Cincinnati, Cincinnati, Ohio 45221-0172, United States;* orcid.org/0000-0003-3902-6876; Phone: 513/556-9222; Email: zhangph@ucmail.uc.edu

William R. Heineman − *Department of Chemistry, University of Cincinnati, Cincinnati, Ohio 45221-0172, United States;* orcid.org/0000-0003-2428-5445; Phone: 513/556-9210; Email: heinemwr@ucmail.uc.edu

Authors

Michael E. Smith − *Department of Chemistry, University of Cincinnati, Cincinnati, Ohio 45221-0172, United States;* orcid.org/0000-0002-4295-8917

Angela L. Stastny − *Department of Chemistry, University of Cincinnati, Cincinnati, Ohio 45221-0172, United States*

John A. Lynch − *Department of Chemistry, University of Cincinnati, Cincinnati, Ohio 45221-0172, United States*

Zhao Yu − *Department of Chemistry, University of Cincinnati, Cincinnati, Ohio 45221-0172, United States*

Complete contact information is available at: https://pubs.acs.org/10.1021/acs.analchem.0c01769

Author Contributions

M.E.S., W.R.H., and P.Z. designed the research project. M.E.S. wrote the manuscript and designed/carried out all experiments and measurements, except for TEM measurements. A.L.S. critically revised the manuscript and provided a program to analyze UV−vis spectra. Z.Y. acquired TEM images of nanoparticle samples. J.A.L. provided technical assistance with the amperometric H_2 sensor.

Notes

The authors declare no competing financial interest.

ACKNOWLEDGMENTS

The authors gratefully acknowledge the National Science Foundation for financial support (NSF ERC 0812348). Dr. Patrick Slonecker is acknowledged for his assistance with gas flow setups.

REFERENCES

(1) Kuhlmann, J.; Witte, F.; Heineman, W. R. *Electroanalysis* **2013**, *25* (5), 1105−1110.

(2) Kuhlmann, J.; Bartsch, I.; Willbold, E.; Schuchardt, S.; Holz, O.; Hort, N.; Höche, D.; Heineman, W. R.; Witte, F. *Acta Biomater.* **2013**, *9* (10), 8714−8721.

(3) Han, H. S.; Loffredo, S.; Jun, I.; Edwards, J.; Kim, Y. C.; Seok, H. K.; Witte, F.; Mantovani, D.; Glyn-Jones, S. *Mater. Today* **2019**, *23*, 57−71.

(4) Zhao, D.; Wang, T.; Guo, X.; Kuhlmann, J.; Doepke, A.; Dong, Z.; Shanov, V. N.; Heineman, W. R. *JOM* **2016**, *68* (4), 1204−1208.

(5) Zhao, D.; Wang, T.; Hoagland, W.; Benson, D.; Dong, Z.; Chen, S.; Chou, D. T.; Hong, D.; Wu, J.; Kumta, P. N.; et al. *Acta Biomater.* **2016**, *45*, 399−409.

(6) Zhao, D.; Wang, T.; Kuhlmann, J.; Dong, Z.; Chen, S.; Joshi, M.; Salunke, P.; Shanov, V. N.; Hong, D.; Kumta, P. N.; et al. *Acta Biomater.* **2016**, *36*, 361−368.

(7) Witte, F.; Kaese, V.; Haferkamp, H.; Switzer, E.; Meyer-Lindenberg, A.; Wirth, C. J.; Windhagen, H. *Biomaterials* **2005**, *26*, 3557−3563.

(8) Witte, F.; Calliess, T.; Windhagen, H. *Orthopade* **2008**, *37* (2), 125−130.
(9) Chakraborty Banerjee, P. C.; Al-Saadi, S.; Choudhary, L.; Harandi, S. E.; Singh, R. *Materials* **2019**, *12* (1), 136.
(10) Song, G. *Corros. Sci.* **2007**, *49* (4), 1696−1701.
(11) Weber, M. J.; Kim, J. H.; Lee, J. H.; Kim, J. Y.; Iatsunskyi, I.; Coy, E.; Drobek, M.; Julbe, A.; Bechelany, M.; Kim, S. S.; et al. *ACS Appl. Mater. Interfaces* **2018**, *10* (40), 34765−34773.
(12) Zhao, D.; Wu, J.; Chou, D.; Hoagland, W.; Benson, D.; Dong, Z.; Kumta, P. N.; Heineman, W. R. *JOM* **2020**, *72* (5), 1851−1858.
(13) Seo, T.; Kurokawa, R.; Sato, B. *Med. Gas Res.* **2012**, *2* (1), 1−6.
(14) Chen, J.; Zhang, J.; Wang, M.; Li, Y. *Sens. Actuators, B* **2014**, *201*, 402−406.
(15) Hussain, G.; Ge, M.; Zhao, C.; Silvester, D. S. *Anal. Chim. Acta* **2019**, *1072*, 35−45.
(16) Jung, D.; Han, M.; Lee, G. S. *ACS Appl. Mater. Interfaces* **2015**, *7* (5), 3050−3057.
(17) Paquin, F.; Rivnay, J.; Salleo, A.; Stingelin, N.; Silva-Acuña, C. *J. Mater. Chem. C* **2015**, *3*, 10715−10722.
(18) Kalanur, S. S.; Lee, Y.; Seo, H. *RSC Adv.* **2015**, *5*, 9028−9034.
(19) Sterl, F.; Strohfeldt, N.; Herkert, E.; Weiss, T.; Both, S.; Giessen, H. *ACS Sensors* **2020**, *5*, 917−927.
(20) Subramanian, S.; Kumar, K.; Dhawan, A. *RSC Adv.* **2020**, *10* (7), 4137−4147.
(21) Chiu, C.; Huang, M. H. *Angew. Chem., Int. Ed.* **2013**, *52*, 12709−12713.
(22) Jiang, R.; Qin, F.; Ruan, Q.; Wang, J.; Jin, C. *Adv. Funct. Mater.* **2014**, *24*, 7328−7337.
(23) Nasir, M. E.; Dickson, W.; Wurtz, G. A.; Wardley, W. P.; Zayats, A. V. *Adv. Mater.* **2014**, *26*, 3532−3537.
(24) Rajoua, K.; Baklouti, L.; Favier, F. *J. Phys. Chem. C* **2015**, *119*, 10130−10139.
(25) Yip, H. K.; Zhu, X.; Zhuo, X.; Jiang, R.; Yang, Z.; Wang, J. *Adv. Opt. Mater.* **2017**, *5*, 1700740−1700753.
(26) Namba, K.; Ogura, S.; Ohno, S.; Di, W.; Kato, K.; Wilde, M.; Pletikosic, I.; Pervan, P.; Milun, M.; Fukutani, K. *Proc. Natl. Acad. Sci. U. S. A.* **2018**, *115* (31), 7896−7900.
(27) Wadell, C.; Nugroho, F. A. A.; Lidström, E.; Iandolo, B.; Wagner, J. B.; Langhammer, C. *Nano Lett.* **2015**, *15* (5), 3563−3570.
(28) Galagan, Y.; Su, W. F. *J. Photochem. Photobiol., A* **2008**, *195*, 378−383.
(29) Shimada, T.; Hasegawa, T. *Spectrochim. Acta, Part A* **2017**, *185*, 104−110.
(30) Harris, D. C. *Quantitative Chemical Analysis*, 7th ed.; W. H. Freeman and Co.: New York, 2007.
(31) Chandrashekar, B. N.; Swamy, B. E. K.; Mahesh, K. R. V.; Chandra, U.; Sherigara, B. S. *Int. J. Electrochem. Sci.* **2009**, *4*, 471−480.
(32) Umeno, M.; Yanagita, K.; Sagami, I.; Shimizu, T. *J. Inorg. Biochem.* **1997**, *67*, 379.
(33) Xu, G.; O'Dea, J. J.; Osteryoung, J. G. *Dyes Pigm.* **1996**, *30* (3), 201−223.
(34) Khazalpour, S.; Nematollahi, D. *RSC Adv.* **2014**, *4* (17), 8431−8438.
(35) Mills, A.; Wang, J.; McGrady, M. *J. Phys. Chem. B* **2006**, *110* (37), 18324−18331.
(36) Oja, S. M.; Guerrette, J. P.; David, M. R.; Zhang, B. *Anal. Chem.* **2014**, *86* (12), 6040−6048.
(37) Porcal, G. V.; Altamirano, M. S.; Glusko, C. A.; Bertolotti, S. G.; Previtali, C. M. *Dyes Pigm.* **2011**, *88* (3), 240−246.
(38) Tratnyek, P. G.; Reilkoff, T. E.; Lemon, A. W.; Scherer, M. M.; Balko, B. A.; Feik, L. M.; Henegar, B. D. *Chem. Educ.* **2001**, *6*, 172−179.
(39) Liu, X.; Chen, T.; Song, P.; Zhang, Y.; Xu, W. *J. Phys. Chem. C* **2018**, *122* (3), 1746−1752.
(40) Han, J.; Zhou, Z.; Yin, Y.; Luo, X.; Li, J.; Zhang, H.; Yang, B. *CrystEngComm* **2012**, *14* (20), 7036−7042.
(41) Caplan, K. J. *Am. Ind. Hyg. Assoc. J.* **1985**, *46* (11), B-10−B-16.
(42) Yu, Z.; Smith, M. E.; Zhang, J.; Zhou, Y.; Zhang, P. *Microchim. Acta* **2018**, *185* (7), 330.
(43) Willets, K. A.; Van Duyne, R. P. *Annu. Rev. Phys. Chem.* **2007**, *58* (19), 267−297.
(44) Christau, S.; Moeller, T.; Genzer, J.; Koehler, R.; Von Klitzing, R. *Macromolecules* **2017**, *50* (18), 7333−7343.
(45) Safety Data Sheet for *N*,*N*-dimethyl-*p*-phenylenediamine. https://www.sigmaaldrich.com/MSDS/MSDS/DisplayMSDSPage.do?country=US&language=en&productNumber=193992&brand=ALDRICH&PageToGoToURL=https%3A%2F%2Fwww.sigmaaldrich.com%2Fcatalog%2Fproduct%2Faldrich%2F193992%3Flang%3Den (accessed 2020-01-07, 2020).
(46) Tran, T. D.; Nguyen, M. T. T.; Le, H. V.; Nguyen, D. N.; Truong, Q. D.; Tran, P. D. *Chem. Commun.* **2018**, *54* (27), 3363−3366.
(47) Gatin, A.; Grishin, M.; Dokhlikova, N.; Ozerin, S.; Sarvadii, S.; Kharitonov, V.; Shub, B. *Nanomaterials* **2019**, *9* (3), 344.
(48) Shim, Y.; Zhang, L.; Kim, D. H.; Kim, Y. H.; Choi, Y. R.; Nahm, S. H.; Kang, C.; Lee, W.; Jang, H. W. *Sens. Actuators, B* **2014**, *198*, 294−301.

https://dx.doi.org/10.1021/acs.analchem.0c01769
Anal. Chem. 2020, 92, 10651−10658